Dual-Frequency Distortion Predictions for the Cutler VLF Array

ERIC C. BERG
University of California, Irvine

MICHAEL A. ROBERTS, Senior Member, IEEE
Veridian

TED L. SIMPSON, Life Senior Member, IEEE
University of South Carolina

The VLF transmitting system in Cutler, ME currently broadcasts at one frequency through a two-element antenna system. This study investigates simultaneous operation at 24.0 and 17.8 kHz. Detailed nonlinear PSPICE models were generated for the system including the amplifier triodes, saturable dynamic-tuning reactors, and the closely-coupled antenna elements. The predicted behavior is in close agreement with available observations. Upper limits are placed on harmonic content, < -59.8 **dBc, and intermodulation distortion,** < -78 **dBc.**

Manuscript received August 15, 2002; revised April 17, 2003; released for publication April 17, 2003.

IEEE Log No. T-AES/39/3/818507.

Refereeing of this contribution was handled by T. R. Roome.

This research was funded under contract N65236-97-D-5806 for the Space and Naval Warfare Systems Center Charleston, Code J535.

Authors' current addresses: E. C. Berg, PO Box 953, Cardiff, CA 92007-0953, E-mail: (eberg@uci.edu); M. A. Roberts, 24436 Del Amo Rd., Ramona, CA 92065-4008; T. L. Simpson, 231 Banbuary Rd., Columbia, SC 29210-4155.

I. INTRODUCTION

The AN/FRT-31 VLF transmitter located at NCTAMS LANT Det Cutler, ME uses two antenna arrays (North and South) and contains four power amplifiers which can be combined in a number of ways. Currently only one frequency is broadcast at a time, with one to four power amplifiers in single or dual antenna array mode. The antenna arrays are identical and located adjacent to each other and are therefore closely coupled. A dual-frequency mode is considered where two power amplifiers operate into each antenna array at different frequencies. A particular concern with this operating mode is intermodulation distortion (IMD) products. IMD products may be generated by the signal from one set of power amplifiers coupling into the other set of power amplifiers. Passing two signals at different frequencies through any nonlinear elements produces new frequencies by mixing the two in various combinations like $(2f_1 - f_2)$. The most significant nonlinear components in the AN/FRT-31 transmitter are the power amplifier triode vacuum tubes and the two saturable core reactors in the antenna tuning networks. To generate intermodulation distortion, the opposing broadcast signal must be induced in the component through the antenna array coupling.

The AN/FRT-31 transmitter and Cutler antenna arrays were modeled in detail by computer using PSPICE as shown in Fig. 1. The voltage sources are applied on the left and pass through the four power amplifiers into the corresponding tank circuits. Two power amplifiers drive the North transmission line, helix house antenna tuning network, and antenna array at one frequency and two other power amplifiers drive the South at a different frequency.

The component models presented herein represent the best models available and were created with considerable study by the authors. MATHCAD, EXCEL, and MININEC were used to generate these detailed component models. PSPICE was then used to implement the models and provide a circuit simulation environment where the analysis took place. Steady state time domain data was generated with PSPICE ("transient analysis") for roughly 100 ms with 1 μs resolution. The model performed in very close agreement with observed behavior of the Cutler VLF system. The analysis established an upper bound for the IMD products expected using the most likely combination of operating frequencies.

II. POWER AMPLIFIERS AND TOROSOLENOIDS

Each AN/FRT-31 power amplifier consists of two sets of five parallel vacuum tubes, connected in a grounded-cathode, push-pull configuration with resonant grid and plate tank circuits. The amplifiers are each rated at 500 kW of RF output power and are operated class C to maximize efficiency. The

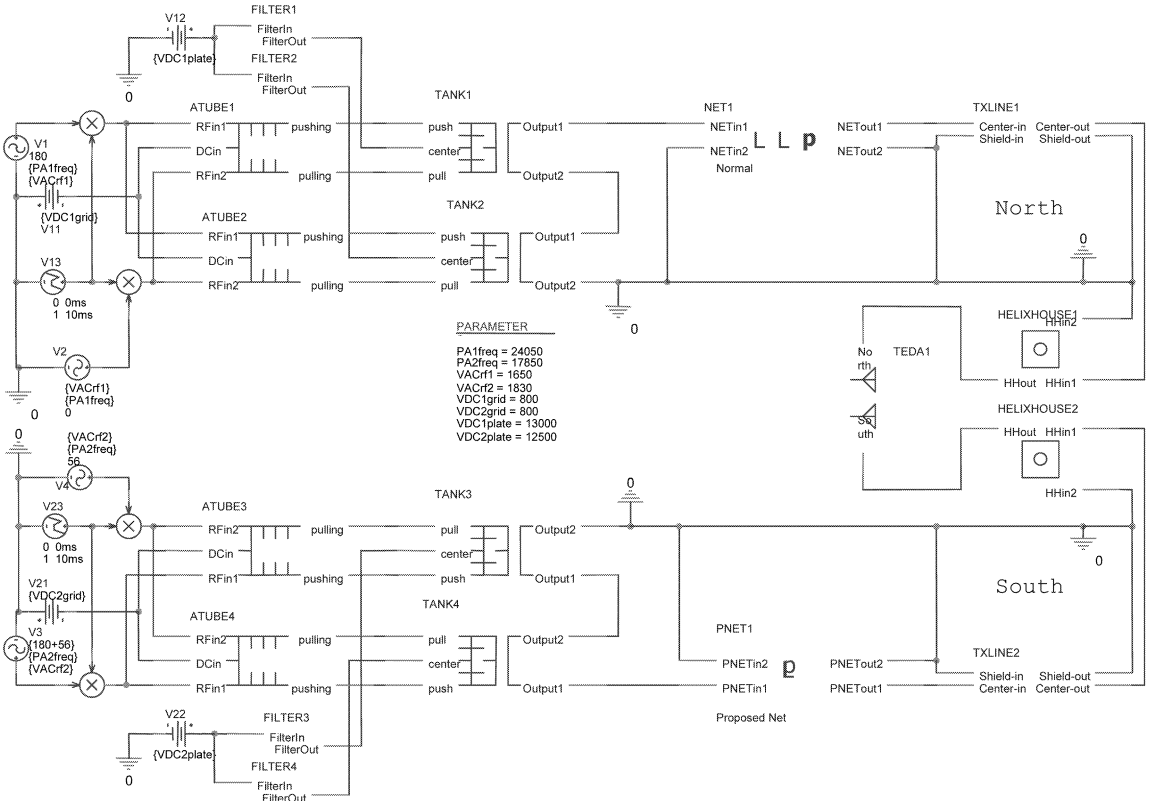

Fig. 1. NTCS Cutler model circuit.

output is coupled with an air-core transformer called a torosolenoid, which has secondary output coils that can be connected in series with another power amplifier to increase broadcast power. The power amplifier load impedance presented by the combiner networks is adjusted to optimize the tube efficiency and output power.

The RF drive to the vacuum tube grids is a minimum-shift-keyed (MSK) RF signal. This is a constant-envelope signal that can be considered a special case of frequency-shift-keying (FSK) with a modulation index of 0.5. The RF drive level is adjusted to bias the tubes to class C operation by means of a grid-leak bias circuit. The RF output power from the amplifier is adjusted by varying the dc plate supply voltage. Two RF drive signals operating 180° out of phase are used to model the North drive as well as the South drive. An arbitrary initial phase difference was applied to the South RF drive relative to the North. When the AN/FRT-31 is first turned on, the RF drives are off and a surge resistor bank is connected in series with the plate power supply filter circuit. The surge resistor bank limits the turn-on current, and minimizes ringing and overshoot of the plate supply voltage. The resistor bank is shorted out by a surge contactor once the filter reaches steady state conditions, to minimize losses in the filter. In the PSPICE implementation it was found that this was unnecessary because the analysis begins with a dc bias point calculation which effectively starts all currents at a first approximation of the steady state value. To reduce ringing of the antenna circuit, the RF drive is ramped up over a period of milliseconds to its final magnitude. In the model this is done between 0 and 10 ms, and found to be sufficiently gradual.

With the exception of the torosolenoids, the model of the power amplifier circuit was constructed directly from the AN/FRT-31 schematics [1] (see Fig. 2). The tube filaments or cathodes are simply connected to ground in the model, whereas the AN/FRT-31 filaments use a separate heating current at RF ground. A diode was added to the 800 V dc grid bias supply to prevent it from sourcing current. The grid tank capacitors $C3$ and $C4$ have discrete values depending on the broadcast frequency, and the variometers (variable inductors) $L1$ and $L2$ are set to resonate with them.

Resistor $R4$ models a metering circuit that displays the grid bias voltage to the transmitter operator, and in practice the RF drive is increased until this meter reads about 950 V. The RF drive levels were set in the model in this way, and verified by waiting for the grid meter voltage to settle ($\sim$ 20 ms). The two frequencies shown in Fig. 1 (17.8 and 24.0 kHz) have different RF drive levels (1830 and 1650 V_{peak}) due to the different circuit Q values as determined by the capacitors $C3$ and $C4$.

The power amplifier circuit loading was studied with PSPICE, and a linear relationship between plate supply current and ideal load resistance was observed

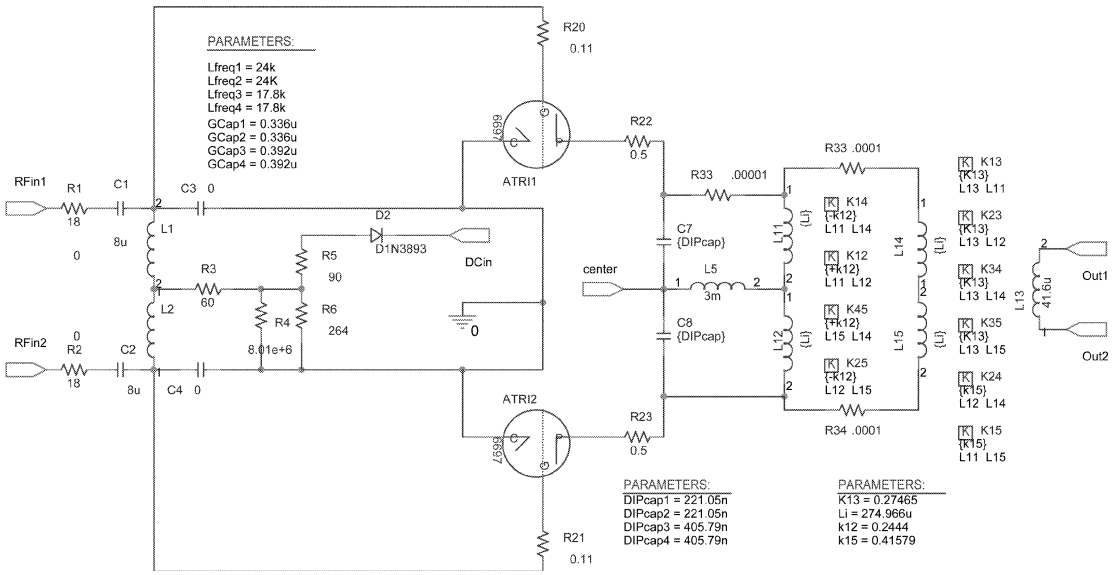

Fig. 2. Power amplifier and tank circuit.

between 57 A and 64 A plate supply current (see (1)). The values of 216 Ω and 59.8 A were selected for the model operating point because the AN/FRT-31 typically operates at 60 A plate supply current. This measured plate-to-plate impedance of $2 * 216$ Ω is very close to the 400 Ω rule of thumb that has historically been applied to this transmitter. The combiner network models were adjusted to provide this impedance as discussed below in Section IV. This operating point was established with a plate supply of 12 kV. This value was later increased (to 12.5 and 13.0 kV for 17.8 and 24 kHz) in order to compensate for inexact network tuning and resulted in 500 kW per power amplifier into the antenna model

$$R_{\text{load}} = -4.0 I_{\text{plate}} + 455.2\ \Omega. \tag{1}$$

In practice the tank capacitors are set by minimizing the plate dc current (i.e. "dipping the plates"), however a model has the luxury of calculating the capacitance needed to resonate the tank circuit exactly. This was done at each broadcast frequency.

The air-core torosolenoid transformers have the unique geometric design of a horizontal toroidal rectangular solenoid with the secondary windings in the shape of vertical infinity bands with the center point at the center of the toroids (see Fig. 3). There are two RF connections and a dc connection on the primary coil and two connections on the secondary, output coil. Although this is a linear component, it requires a detailed model due to the unique geometry. The primary coil has 52 turns evenly arranged around the toroid. The windings are reversed on the left and right halves (as shown) so that current from both sides contributes to the flux in all quarter elements. The secondary coil has 8 turns, half around each side of the toroid wound in opposing directions. The

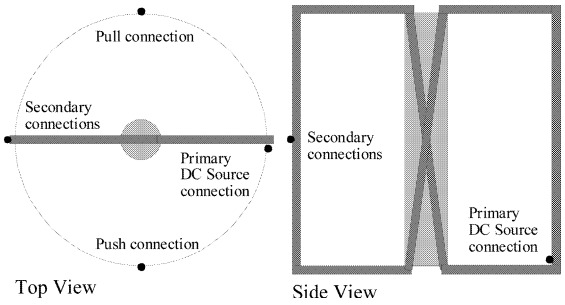

Fig. 3. Torosolenoid geometry.

air-core dimensions are: inner radius = 15 in, outer radius = 48 1/8 in, and height = 95 3/4 in [28]. The primary, secondary, and overall mutual inductances were available from historical measurement data [3]. A value of 389.3 μH was used for the measured primary inductance, the secondary inductance was measured to be 41.6 μH, and the overall mutual was found to be 58.75 μH.

For our model, the toroid was divided into four quadrant coils, labeled 1 through 4 clockwise from straight up as shown in Fig. 3. The secondary was labeled coil 5. Since equipment operational requirements precluded access for electrical measurements, the challenge became one of determining these 5 inductances and 10 coupling constants from only three electrical measurements and the coil dimensions. Because there are geometric symmetries, the inductances $L_1 = L_2 = L_3 = L_4$, and the coupling constants $k_{12} = k_{34}$, $k_{14} = k_{23}$, $k_{13} = k_{24}$, and $k_{15} = k_{45} = k_{35} = k_{25}$. L_5 was measured. Due to the solenoid's opposed windings on each half, $k_{14} = -k_{12}$. This reduces the calculation to four unknowns: L_1, k_{12}, k_{13}, and k_{15}. The overall primary inductance measurement was performed with the dc source connection floating, so the voltage across either side

of the primary was equal. Equation (2) can be derived by considering all the mutual inductances among the four quadrants

$$k_{13} = L_{\text{primary}}/L_1 - 1. \tag{2}$$

The inductance of "coil 1 plus coil 2" is the sum of L_1, L_2 and twice the mutual between them. Also, the inductance of a straight solenoid is proportional to the number of turns squared times the diameter, and the construction of the torosolenoid is such that the flux is distributed as if the solenoid were straight. Because the diameters are the same for "coil 1 plus coil 2" and coil 1 and 2 considered separately, the relationship in (3) involves only the proportionality constants, F_{12} and F_1, respectively

$$k_{12} = 2(F_{12}/F_1) - 1. \tag{3}$$

The quadrant inductance, L_1 can be calculated given that there are 52/4 turns. The diameter and length can be estimated and used to graphically solve for the proportionality constant F_1 [16]. The midpoint between inner and outer toroid radii was used to determine the length of the quadrant equivalent solenoid to be 49.578 in. The diameter of the solenoid was estimated by averaging the distance from the center over the rectangle to be 72.312 in. The graphically solved proportionality constants are $F_{12} = 0.014$ and $F_1 = 0.0225$. The coupling to the secondary, k_{15} was set by adjusting it until the coupling from the primary to the secondary matched the measured value of 58.75 μH. The final values are listed in (4). The PSPICE model was constructed with these five inductors and ten coupling constants and reproduced the primary overall inductance as expected (see Fig. 2)

$$\begin{aligned} &L_1 = L_2 = L_3 = L_4 = 274.966\ \mu\text{H} \\ &L_5 = 41.6\ \mu\text{H} \\ &k_{12} = k_{34} = -k_{14} = -k_{23} = 0.2444 \\ &k_{13} = k_{24} = 0.41579 \\ &k_{15} = k_{45} = k_{35} = k_{25} = 0.27465. \end{aligned} \tag{4}$$

III. TRIODES

The AN/FRT-31 power amplifiers use Eimac 6697 triode vacuum tubes. The plate current and the grid current are not simple linear functions of the applied voltages, and this nonlinear characteristic is essential to the high-efficiency class C operation. This nonlinearity is the only significant source of harmonic and intermodulation distortion in the amplifers. The tubes are connected with the cathodes grounded. Typical interelectrode capacitances have been specified by the manufacturer [6, 7] to be: grid-plate = 55 pF, grid-filament = 76 pF, and plate-filament = 2.7 pF. The nominal amplification factor (μ) of 20 provides a starting point for modeling, and a fit to the manufacturer's typical grid and plate current as a function of grid and plate voltage shows the model's limits.

A variety of published triode modeling equations and combinations were fit to the manufacturer's instantaneous plate current curves (sampled at 132 points). A χ^2 minimization was used with Microsoft EXCEL Solver (as suggested by [25]) to aid in determining the best model parameters. The quality of the model was estimated by calculating an average uncertainty in the grid voltage, for a given plate current and plate voltage, such that the agreement was statistical at the 90% confidence level (assuming Gaussian errors). The average uncertainty was determined from the sqrt(χ^2/degree of freedom) adjusted by a factor close to 1.0 which brought the confidence level to 90% [26]. A larger average uncertainty in the grid voltage, $\langle dV_g \rangle$, indicated a poorer model fit to the manufacturer's measured data. Equation (5) defines the best plate current model

$$\begin{aligned} \mathbf{I}_p = \{(V_p + 137)/[279(V_p + 582)]\}\{[(V_p + 137)/316]^* \\ \times \ln[1 + \exp(316[1/21.58 + V_g/(V_p + 137)])]\}^{1.467}. \end{aligned} \tag{5}$$

The procedure for modeling the grid current was the same, however positive grid current and negative grid current were considered separately. The manufacturer's curves were sampled at 18 and 16 points for model comparison, respectively. Equation (6) defines the best model for positive grid current

$$I_g = (V_g - 78 - 0.0466V_p^{1.085})/67. \tag{6}$$

Equation (7) defines a new phenomenological model for negative grid current that matches the tube characteristics very well, with a value of $\langle dV_g \rangle = 0.2$ V. This equation is noninvertable; it cannot be solved for $I_g(V_g, V_p)$, and so cannot be simply implemented in PSPICE. Because normal operation of these amplifiers should never produce negative grid current, (7) was not included in our model

$$\begin{aligned} \mathbf{V}_p = 3.75(V_g + 270^* I_g^2 - 470^* I + 384) \\ + 1000(400/(V_g - 43^* I_g^2 + 63^* I_g - 132))^{-0.531}. \end{aligned} \tag{7}$$

Table I summarizes the models examined, best-fit parameters, and corresponding average grid voltage uncertainties for the plate current and positive grid current models.

Equations (5) and (6) were implemented in PSPICE with the ABM (analog behavior model) parts in CAPTURE, a schematic interface and front end for PSPICE. The AN/FRT-31 power amplifiers use ten tubes each with two groups of five parallel tubes arranged in a push-pull configuration. A test was done comparing a model of an array of ten tubes with

TABLE I
Triode Models

#	Plate Current Models	Refs	Best Fit Parameters	$\langle dV_g \rangle$
1	$I_p = K(V_g + V_p/\mu)^{3/2}$	12, 13	$\mu = 19.67$, $K = 0.00238$	25.9 V
2	$I_p = K(1 + V_g/(B - V_g/C))(V_g + V_p/\mu)^{3/2}$	11	$\mu = 19.9$, $K = 0.00123$, $B = 0$, $C = -1$	>25.9 V
3	$I_p = K(V_p/(V_p + C))(V_g + V_p/\mu)^{3/2}$	11	$\mu = 19.9$, $K = 0.00254$, $C = 160$	poor at large I_p, low V_p
4	$I_p = (E_1^{E_x})/K_{g1}$ where $E_1 = V_p/K_p \ln(1 + \exp(K_p(1/\mu + V_g/\mathrm{sqrt}(K_{vb} + V_p^2))))$ $E_x = aV_p^3 + bV_p^2 + cV_p + d$	8, 9, 10	$K_{g1} = 340$, $K_p = 310$, $\mu = 21.3$, $K_{vb} = 500000$, $a = 0$, $b = 0$, $c = 0$, $d = 1.492$, (can't solve for a, b, c)	excellent for $V_p > 4$ kV, too steep at low V_p
5	$I_p = K \tanh(V_p/B)(V_g + V_p/\mu)^a$	15	$K = 0.00244$, $B = 600$, $\mu = 19.81$, $a = 1.5$	25.0 V
6	$I_p = (1/K_{g1})((V_p + E)/(V_p + C + E)E_1^{E_x}$ $E_1 = (V_p + E)/K_p \ln(1 + \exp(K_p(1/\mu + V_g/\mathrm{sqrt}(K_{vb} + (V_p + E)^2))))$ $E_x = a(V_p + E)^3 + b(V_p + E)^2 + c(V_p + E) + d$	mix 3+4	$K_{g1} = 279$, $C = 445$, $K_p = 316$, $\mu = 21.58$, $K_{vb} = 0$, $a = 0$, $b = 0$, $c = 0$, $d = 1.467$, $E = 137$	18.0 V
7	$I_p = (\tanh((V_p + E)/B)/K_{g1})E_1^{E_x}$ $E_1 = (V_p + E)/K_p \ln(1 + \exp(K_p(1/\mu + V_g/\mathrm{sqrt}(K_{vb} + (V_p + E)^2))))$ $E_x = a(V_p + E)^3 + b(V_p + E)^2 + c(V_p + E) + d$	mix 4+5	$B = 1100$, $K_{g1} = 600$, $K_p = 363$, $\mu = 20.92$, $K_{vb} = 0$, $a = 0$, $b = 0$, $c = 0$, $d = 1.571$, $E = 275$	19.8 V
#	Positive Grid Current	Refs	Best Fit Parameters	$\langle dV_g \rangle$
1	$I_g = G((V_g + E)^{3/2})((A + V_p)/(B + V_p))^4$	11	$G = 0.05$, $A = 130$, $B = 1000$, $E = -219$	237 V
2	$I_g = (K - C \tanh(2.5V_p/B))(V_g + V_p/\mu)^A$	14	$K = 0.00058$, $C = 0.00045$, $B = 4400$, $\mu = 100$, $A = 1.527$	88.3 V
3	$I_g = (V_g - B - CV_p^A)/K$	Berg	$B = 78$, $C = 0.0466$, $A = 1.085$, $K = 67$	31.1 V

a model of two modified tubes. The modifications combined the tube capacitances and currents in parallel as well as the power amplifier resistors, effectively contributing a factor of five. The test showed that both models produced identical results, yet the ten-tube array model took four times longer to run. For this reason the combined tube model was used for this analysis.

For the final analyses, elliptical load lines (see [27]) were plotted for plate current and found to lie within the region sampled and fit. This comparison is shown in Fig. 4, including the negative grid current which was not included in the PSPICE circuit. The lower majority of the load lines fall in a region with zero plate current; indeed the conduction angles of 103°, 116°, and 108° for 24, 23.95, and 24.05 kHz, respectively, are consistent with the tube operation in the AN/FRT-31. The upper left corner of the load lines are in a region of less than ideal agreement between models and specifications, however the amount of time spent there is small, reducing errors in the predictive ability of the models.

IV. COMBINERS, TRANSMISSION LINES AND TUNING NETWORKS

The AN/FRT-31 power amplifiers, generally speaking, each require about 9 Ω of real load impedance plus a capacitive reactance to cancel the 41.6 μH self-inductance of the torosolenoid secondary coils. The combiners provide this load, serve as switchgear for connecting one to four power amplifiers to one or both antenna arrays, match the transmission line impedance, and introduce enough phase delay in the current so that there is a multiple of 90° between the antenna array and the triode plates. This phase relationship ensures that the plate antenna currents are symmetric with modulation between the two MSK shift frequencies. The phase delays are about 25° for the transmission lines, 273° for the antenna tuning networks, and 82° for the tank circuits. Therefore the required phase delay for the combiners is about 70° (or 160°). The characteristic impedance of the transmission lines is 100 Ω. The antenna tuning networks cancel the capacitive reactance of the antenna arrays forming a resonant circuit at the broadcast frequency, convert the antenna array resistance to 100 Ω to match the transmission line, and introduce a phase delay close to a multiple of 90°.

Presently the AN/FRT-31 includes a normal combiner network and an emergency combiner network. The emergency combiner approximates the impedance and phase delay requirements and provides limited switching. Operation in the proposed dual-frequency mode would require a new combiner

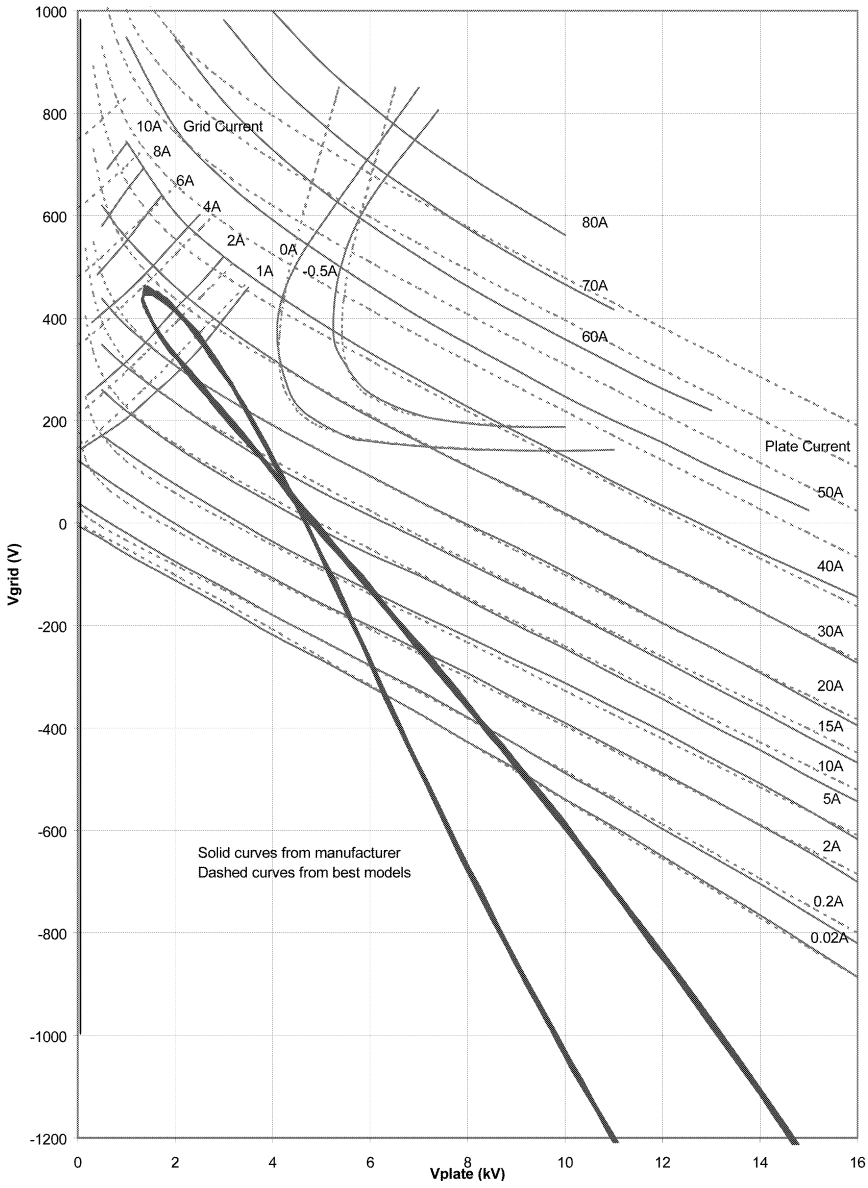

Fig. 4. Triode results. (*Bold curve is road line.*)

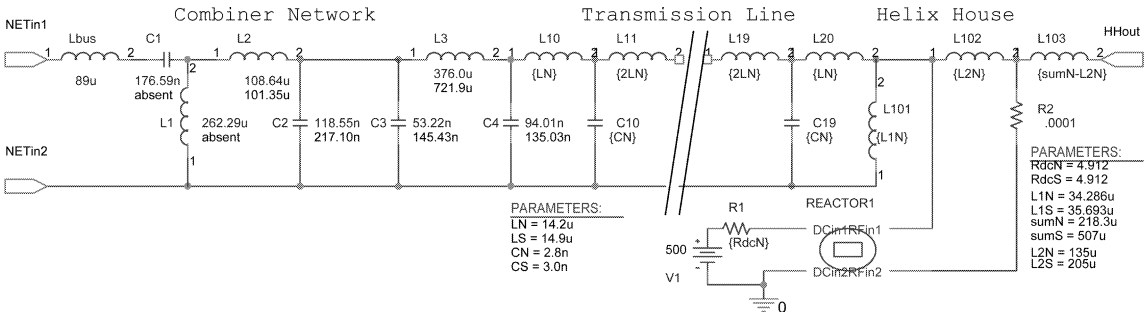

Fig. 5. Combiners and antenna tuning networks.

for a second frequency. This would allow two power amplifiers to drive the North antenna array independent of the other two power amplifiers driving the South antenna array. For this study we consider the normal combiner network and a simpler proposed combiner network, which could incorporate components of the emergency combiner (see Fig. 5). The normal combiner is described in several places [1, 4, 23, 35], and consists of a π-network with switching to provide for single or dual antenna array

single frequency operation, and two L-networks with switching to accommodate multiple power amplifier operation. The π-network transforms the 100 Ω load impedance to 36 Ω input impedance, as well as contributes the required phase delay. The two L-networks transform the 36 Ω to 18 Ω as required for two power amplifier operation.

The proposed second combiner topology is simpler, consisting of one L- and one π-network, which provide less filtering. Our model indicates that the greatest source of radiated harmonics are from the saturable reactors (see Section V) and not the triodes, so increased filtering in the proposed combiner would not significantly reduce the broadcast harmonic energy [21].

The combiner networks were constructed and modeled with simple analog inductors and capacitors. Component values for the PSPICE models were calculated using the gross resistance of the antenna model, which differed slightly from the measured gross resistance. The impedances at the L-networks and the π-network were verified in the model at 24 kHz, and the overall impedance was $18.055\ \Omega - j2\omega 41.9\ \mu$H, which is close to canceling the torosolenoid secondary's 41.6 μH impedance.

The phase delay of the current in the model from the triode plates to the corresponding antenna bushing was measured and found to be slightly different from a multiple of 90° due to approximations in the combiner calculations. The antenna current symmetry between high and low 200 baud modulation shift frequencies (i.e. $\pm$50 Hz) was then checked and found to be slightly asymmetric. A slight increase in the first series capacitance $C1$ in the North, and a slight decrease in the first series inductance $L4$ in the South were required to make the antenna current symmetric. This adjustment is seen in practice with the AN/FRT-31, suggesting that the models are quite accurate.

The transmission lines have been measured electrically several times. An older study reported the derived physical lengths as North = 834 m and South = 875 m [22]. These numbers were quoted in a more recent study as North = 2735 ft and South = 2870 ft [23]. The most recent measurement [3, 4] reports the frequency dependent phase delays as North = $-1.026f$ (in kHz) + $0.05 \pm 0.1°$, and South = $-1.079f$ (in kHz) $- 0.07 \pm 0.1°$, as well as the characteristic impedances as Z_0 (North) = 100.1 Ω and Z_0 (South) = 100.0 Ω. These measured delays correspond to lengths of 2761 ± 11 ft in the North and 2904 ± 11 ft in the South, which are statistically consistent with the earlier ones at the 23% confidence level. The more recent measurement, however, was believed to have less systematic measurement bias and was therefore used for our model. The manufacturer specifies the transmission line's velocity factor v_f as 0.985 and characteristic impedance Z_0 as 100 Ω [30]. They also specify that the intermodulation distortion *produced* in these transmission lines is very small. For a similar product the manufacturer sets the relative magnitude at -163 dBc independent of frequency [31]. The attenuation in the line is also very small, due to the large diameter (9 in) and low frequency of operation. A loss-less lumped element model of this transmission line is simple to construct and is adequate for our analysis. A series of ten T-networks consisting of series inductors and shunt capacitors was sufficiently distributed to provide excellent results. The resulting T-network element values that correspond with the North and South transmission line data are $L_{\text{North}} = 14.2\ \mu$H, $C_{\text{North}} = 2.8$ nF, $L_{\text{South}} = 14.9\ \mu$H, and $C_{\text{South}} = 3.0$ nF. When the model was tested at 24 kHz, the characteristic impedances were found to be $Z_0(\text{North}) = 00.23 + j0.53\ \Omega$ and, $Z_0(\text{South}) = 98.10 + j2.12\ \Omega$. The phase delays were found to be $\phi_N = 24.22°$ and $\phi_S = 25.76°$ which agree well with the measured values of 24.67° and 25.83°.

The antenna tuning network circuit for the North and South identically consists of a tuning helix that can be tapped at various points (n-turn coils), a tuning variometer with a range of 60–220 μH, a variable coupling coil, and a saturable reactor (see Section V). The interconnecting bus inductance is on the order of 25 μH and there are some stray capacitances on the order of 100 pF. For the present Cutler operating configuration, the transmission line is shunted by the coupling coil, and then connected to the tuning variometer and reactor in parallel, before passing to the helix in series. Configurations have been proposed for optimal operation with a reactor at 17.8 and 24.0 kHz [5]. For the purpose of this analysis, our model used a simplified configuration of linear elements: a shunt coupling coil, followed by a reactor in parallel with an variable inductor, followed by a second variable inductor. In tuning the network for a given frequency, the coupling coil was adjusted to provide 100 Ω input impedance ($\pm 1\ \Omega$), the inductance in parallel with the reactor was set to provide a $\pm$50 Hz tune shift ($\pm$5 Hz) due to the reactor operation between 33 A and 97 A, and the remaining series inductance was set to tune the antenna array to center frequency ($\pm$1.5 Hz).

V. SATURABLE REACTORS

The AN/FRT-31 antenna tuning circuits use saturable reactors that dynamically adjust the antenna tuning synchronized with frequency shifts of the MSK broadcast signal. The tuned antenna array has a narrow bandwidth relative to the frequency separation between the two MSK shift frequencies, which causes data ambiguity and reduces the maximum radiated power. To compensate, an inductor is needed that can change values in about a millisecond. The saturable reactors provide this function by switching

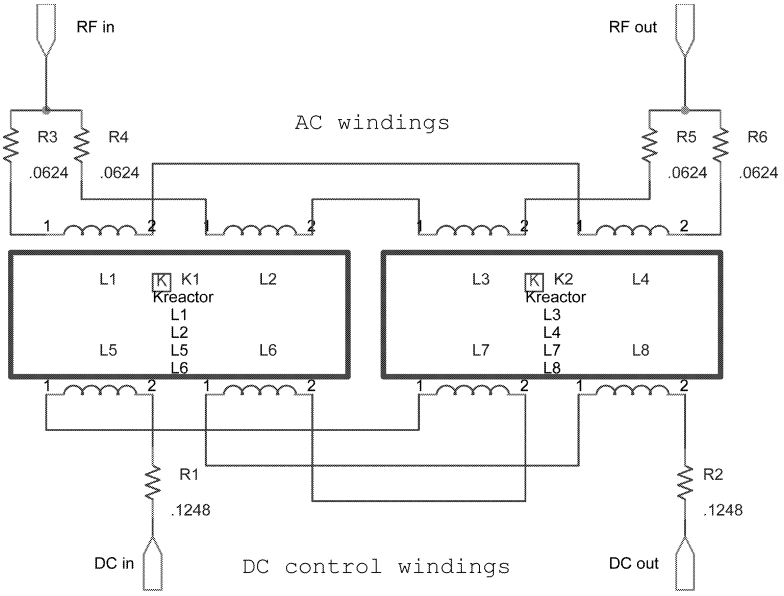

Fig. 6. Saturable reactor circuit.

between two levels of magnetic core saturation using two levels of dc control coil current. As the cores become more saturated, the permeability is decreased, resulting in lower inductance. With a reactor switching inductance between two values, the antenna tuning circuit resonance can be made to track the broadcast signal frequency, thereby mitigating the effects of the narrow bandwidth.

The reactors are very nonlinear and together with the triodes are the only significant nonlinearities in the entire circuit. These nonlinearities are the principal sources for intermodulation distortion, and together with the antenna array coupling are the key factors in this analysis.

The saturable reactors at Cutler were made by Westinghouse at least 40 years ago and are simply transformers with ferrite cores. The circuit diagram in Fig. 6 shows how the coils are connected to reduce RF induction in the control windings by connecting the control windings in a bucking configuration. The coil resistances were measured as indicated. The cores consist of multiple offset layers of stacked bricks. The mean magnetic cross sectional AREA and the mean magnetic PATH length are available from the core drawings [20]. The effective air GAP and the stacking or lamination factor (PACK), however, are not indicated on the drawings and had to be estimated. All of these values are listed in Table II.

The accepted theoretical model for isotropic nonlinear magnetic cores is called the Jiles-Atherton model and is defined by (10) [17, 38]. The material parameters are defined as follows. MS is the saturation magnetization, A^* is the modified Langevin anhysteretic curve parameter, K^* is the domain wall pinning strength, C is the reversable magnetization strength or domain wall flexing parameter, and

TABLE II
Reactor Model Parameters

Parameter	Best Fit	At 25°C	At 100°C
MS (A/m)	—	298,000 to 414,000	167,000 to 294,000
A* (A/m)	—	6 to 114	4 to 58
K* (A/m)	—	11 to 136	10 to 90
C	—	0.12 to 0.97	0.22 to 0.92
α	—	0.08e-4 to 6.4e-4	0.15e-4 to 5.0e-4
AREA	723 cm^2	—	—
PATH	438 cm	—	—
GAP	0.20 cm	—	—
PACK	1.0	—	—
MS	430,000 A/m	—	—
A	800 A/m	—	—
K	100 A/m	—	—
C	0.92	—	—

α is the interdomain coupling strength. PSPICE implements this model using a simplified anhysteretic function that does not use the parameter α, and is defined by (11) [19]. Here the PSPICE K and A parameters are redefined as the domain anisotropy parameter and the thermal energy parameter, and differ considerably from the Jiles-Atherton K^* and A^* parameters

$$\frac{dM}{dH} = \frac{(M_{an}-M)}{(1+C)[\delta K^*/\mu_o - \alpha(M_{an}-M)]} + \frac{C}{(1+C)}\frac{dM_{an}}{dH} \tag{10}$$

$$M_{an} = M_s[\coth(H+\alpha M/A^*) - (A^*/H+\alpha M)]$$

$$\frac{dM}{dH} = \frac{(M_{an}-M)}{(1+C)K} + \frac{C}{(1+C)}\frac{dM_{an}}{dH} \tag{11}$$

$$M_{an} = M_s(H/(|H|+A)).$$

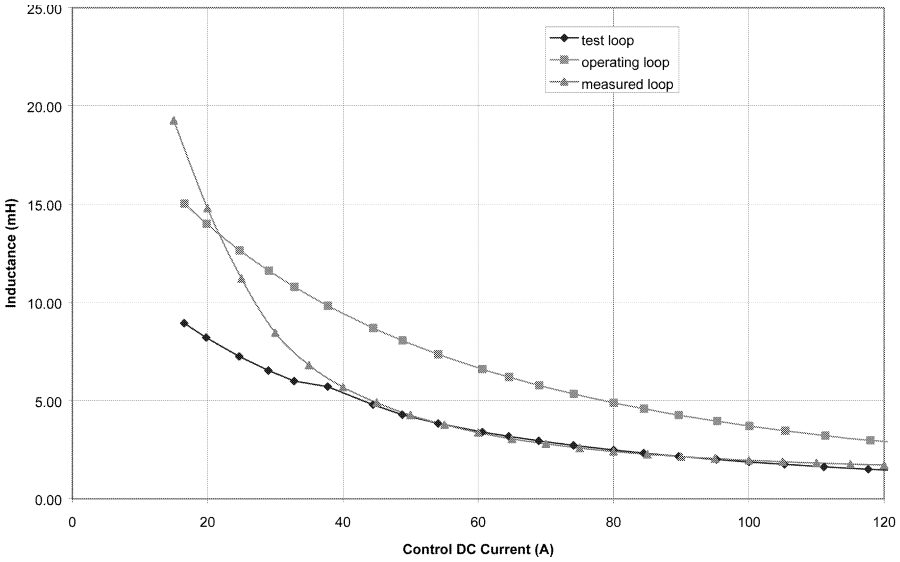

Fig. 7. Saturable reactor inductance (24.0 kHz).

The core material is Type III Ferroxcube by Phillips. Unfortunately, specifications for this material cannot be located. Several references have been found which describe the slightly newer materials called Type IIIA, IIIB, IIIC, and IIID, as well as present day materials like 3C08, 3C81, and 3B7 [39–43]. The Type IIIA, IIIB, IIIC, and IIID materials have values of MS from 267,000 to 406,000 (A/m) at 20°C and Curie temperatures from 130 to 235°C [41]. The present day materials have been studied extensively and Jiles-Atherton parameters are specified for them (see Table II) [20]. Notice the large temperature sensitivity. Reference [43] states also that Type III has a high degree of temperature sensitivity. At Cutler, a seasonal variation should be noticeable as the ambient temperature varies considerably, resulting in reactor temperatures of about −15°C to 40°C. Particular care should be exercised when comparing measurements made at lower temperatures to operating conditions at higher temperatures. It might be assumed that these materials are similar to the original Type III used in the AN/FRT-31, however the initial permeability of Type III is known to be significantly different from any of these materials [42]. Therefore, without testing the core material itself, only the order of magnitude can be estimated for these parameters. Values were set in the model based on comparison with the few measurements available as described below.

The reactor circuits were implemented in PSPICE with inductor parts and coupling parts [36]. PSPICE provides a linear core coupling (K_LINEAR) and many nonlinear cores (MAGNETIC.OLB), but not the cores at Cutler. PSPICE also provides a custom core part (KBREAK), which interprets the value of an inductor as the number of turns rather than the inductance. The value of the coupling constant for KBREAK should never be less than 0.9 or else the PSPICE implementation may fail [37], and so our model used a fixed coupling of 1.0. Often it is useful to perform an ac sweep analysis, so that the tune frequency can be quickly measured. The PSPICE implementation of an ac sweep analysis linearizes the circuit, and so with this analysis type, the KBREAK part effectively becomes K_LINEAR [37]. Unfortunately, PSPICE linearizes KBREAK at zero saturation. Therefore all measurements of the reactor model were made with a transient analysis. It is important to note that in PSPICE the transient analysis does not calculate certain variables such as the phase between two waveforms, and such measurements were made by visual comparison.

PSPICE provides a powerful program for generating model parameters called the MODEL EDITOR. However, because the hystersis curve of Type III material is not now known, the MODEL EDITOR cannot be used. Instead, the reactor circuit was used and the model parameters were varied by hand until a good agreement was found with the measurements from [3] [18] (see Fig. 7). The RF coil inductance was measured at ~ 15°C by using a 38 V rms RF source and various dc coil currents [3]. Each model inductance value was determined with a transient analysis using data after the transient response had diminished (~ 20 ms with a 500 V dc control winding supply). The region between 33 A and 97 A dc current was of particular interest since these are the values presently used in the AN/FRT-31 at 24 kHz. The resulting best fit parameters are given in Table II, where variations in AREA, PATH, and PACK were not investigated. Nothing could be done to adjust the model to normal operating temperature operation because no data exists as to the magnitude this effect has on the inductance. The measured inductances also differ from the operating inductances

TABLE III
Harmonic Distortion From Reactor

	Measured		Model	
Frequency (kHz)	With Reactor	Without Reactor	High dc current	Low dc current
17.8	0 dBc	0 dBc	0 dBc	0 dBc
53.4 – 3rd	−59 dBc	−71 dBc	−57.0 dBc	−70.2 dBc
89.0 – 5th	−80 dBc	−83 dBc	−78.6 dBc	−87.3 dBc
124.6 – 7th	−88 dBc	−92 dBc	−79.7 dBc	−86.8 dBc

because they are effective averages over an RF cycle's hysteresis loop, which differs in shape with RF magnitude. The model predicts that the operating inductances are about twice as large as that for a 38 V rms test signal (see Fig. 7). Observations have shown that the difference is small, however there was no clear way to improve the model without additional measurements of the existing reactor.

The RF noise on the dc coil has been observed to be substantial ($\sim \pm 15$ A [3]), however the model predicts a negligible amount (~ 2 mA). It is believed that the number of turns on each winding is not precisely the same (43) and this is the explanation for the induced RF voltage. That is, there are fractional turns due to hookup leads, and this unbalance would introduce additional coupling that would not be canceled by the counter-wound coils.

Measurements of the AN/FRT-31 have shown that the presence of the reactor in the tuning circuit produces harmonic distortion in the antenna current. This is also seen in the model at about the same magnitudes. Table III compares measured harmonic distortion with model values [21]. The measurements were made with modulation (i.e., alternating between the two dc current values), so the "with reactor values" should be close to half power (−3 dBc) of the "high dc current" values, and the "without reactor values" should be less than the "low dc current values." Indeed this is within 1 dB, 4 dB, and 5 dB of what is observed for 3rd, 5th, and 7th harmonics.

VI. ANTENNA ARRAYS

The AN/FRT-31 antenna arrays consist of two identical heavily top-loaded, electrically short monopoles. The arrays are called the North and South antenna arrays and are strongly coupled due to their proximity. We describe here the development of an equivalent circuit to simulate the electrical interaction between the two separate Cutler antenna arrays as a linear two-port electrical circuit. The primary criterion used in the design of this equivalent circuit was to minimize the discrepancy between available information, both from measurements and from theory, on the impedance spectrum and that predicted by the equivalent circuit under study. In addition, to support the prediction of intermodulation resulting from operating the two arrays at different frequencies, the bandwidth for accurate simulation by the equivalent circuit should extend from 15 to 90 kHz to include up to the third harmonic of the highest frequency of the conventional VLF band (15–30 kHz).

Three types of impedance data were available for use as comparative standards in the creation of an equivalent circuit for the two-array Cutler antenna system.

1) Early predictions of the impedance variation were based upon a simple series RLC circuit or, more accurately, upon such a circuit augmented by the addition of a small capacitance (C_s) shunted across the input yielding a π-circuit. Hansen [4] summarizes this approach.

2) Measurements were recently made of the input impedance to both the North and South arrays with the unused array grounded. The most recent and complete set of such data was obtained by Beauchamp, Gish, and Hopkins [22, 23], although some earlier measurements of resistance obtained by Raudenbush [35, 44] were also found to be useful. In addition, the mutual impedance between the two arrays was measured by Watt and Smith [45] at two important frequencies, 17.8 and 24 kHz.

3) Theoretical calculations were made for even- and odd-mode excitation (i.e., the North and South arrays were driven with equal and opposite input voltages) using MININEC, a program that uses the method of moments. From this analysis, three types of impedance spectra were obtained: a) even-mode, or dual-array, impedance, b) single-array impedance with "off" array grounded, and c) mutual impedance. The theoretical results filled a real need since no direct measurements of the dual-array impedance, and only two values of the mutual impedance were available. This analysis, carried out by Simpson in 1997 at NCCOSC (Naval Command, Control and Ocean Surveillance Center), has not appeared previously in print.

In the simplest approach to an equivalent circuit, Hansen's π-circuit [4], the bulk of the capacitance (C_a) is attributed to the extensive top loading; the near-base capacitance (C_s) to the numerous downlead busses fanning out horizontally from each helix house to the vertical dowleads; the inductance (L_a) being thought of as associated with the current concentrated in the six vertical downlead busses. The resistance (R) is primarily due to radiation with a small additional loss component. In the course of the present study it was found that a fairly accurate model for single-array operation could be obtained by shunting the inductance L_a with a resistance of approximately 1.4 kΩ. This circuit yields an input impedance that agrees very well with measured results.

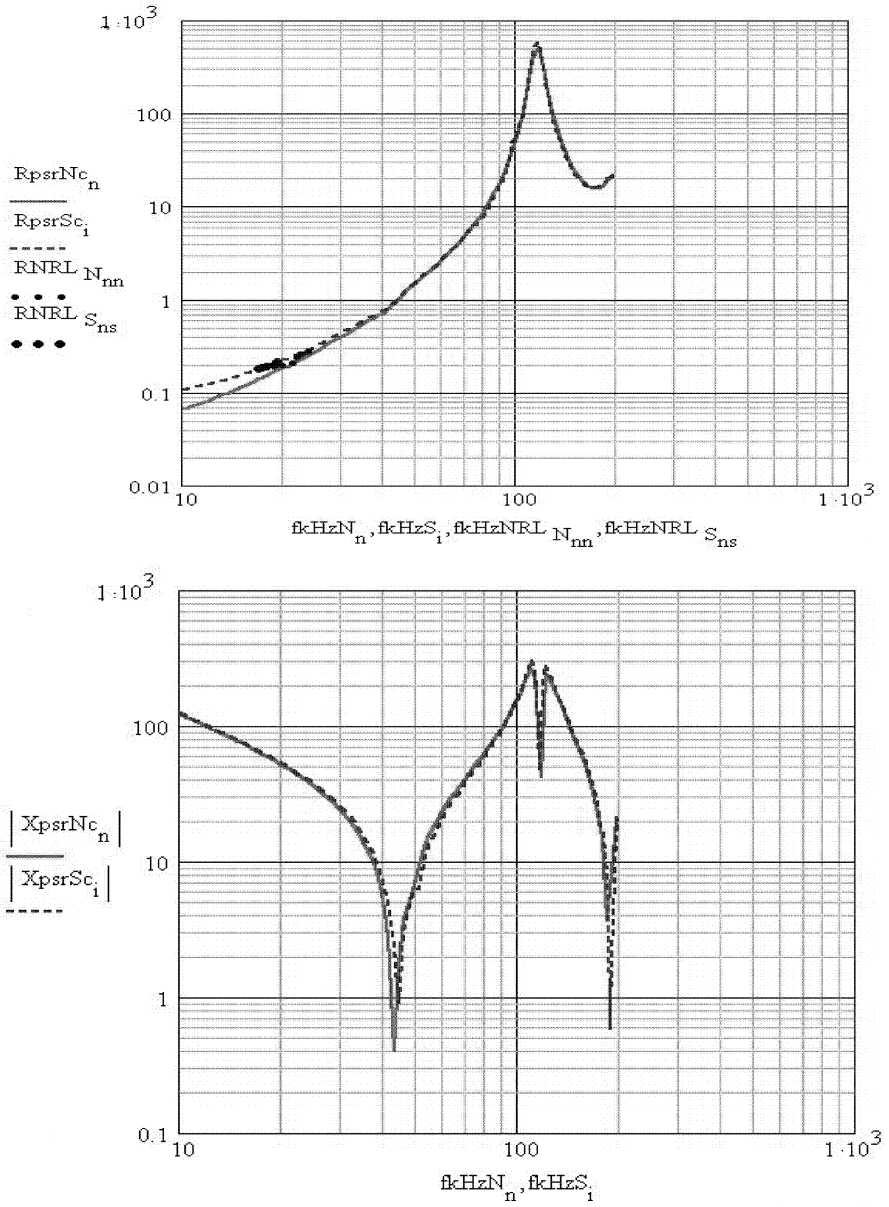

Fig. 8. Single-array measured resistance and reactance.

Measurements by Beauchamp, Gish, and Hopkins [22, 23], of the input impedance of both the North and South arrays extend from 10 kHz to 200 kHz. The magnitude of the impedance, obtained using a network analyzer at fairly low power, is in substantial agreement with the terminal impedance predicted using a π-circuit described by Hansen [4]. This gave good definition to the dominant component, the reactance, but only a rough indication of the resistance, especially at the lower frequencies where the resistance is only a fraction of an ohm. To improve the usefulness of this data for use as a comparative standard in circuit development, the data was smoothed in places where it was obviously contaminated by noise spikes. It was also augmented by manually filling in a smooth curve for the resistance versus frequency consistent both with such values of resistance as seemed well defined and with the theoretical resistance curves. Since the theoretical MININEC model did not include ohmic losses, this required some judicious extrapolation. Fortunately, the North data was considerably less noisy than the South data, so that the input resistance of at least one array was fairly well defined by direct measurement. Early measurements by Raudenbush [35, 44] indicated a significantly greater gross input resistance for the South array as opposed to that for the North, and the extrapolated curves sketched in for the resistance of the South array were intentionally distorted, so to speak, by the addition of ohmic resistance to the theoretical for the South resistance. Whether or not this difference between the two arrays is true at

operating power levels, as opposed to measurement levels, remains to be determined. Hansen [4] discusses this point, attributing this anomaly to the presence of insulator leakage current on damp insulators at low power, an effect unlikely to be present in full-power operation.

In the course of analyzing their results, Beauchamp, Gish, and Hopkins [22, 23] found that a correction was required to account for a test lead inductance of 29.5 μH for the North array and 26.8 μH for the South array. After correcting for this excess inductance, and smoothing and interpolating as discussed above, the single-array impedance profiles shown in Fig. 8 were obtained. Here, RpsrNc and RpsrSc refer to the resistance measured and corrected by Pacific-Sierra Research (PSR) for the North and South arrays, respectively, and XpsrNc and XpsrSc refer to the reactance measured by PSR, again for the North and South arrays. This body of data was used as the fundamental standard against which candidate equivalent circuits were compared. At low frequencies, where it is well known that the radiation resistance for even-mode excitation essentially doubles at each of the two input terminals, the resistance in Fig. 8 was doubled for comparison with the even-mode equivalent circuit impedance. While this is only approximate, since the ohmic loss component remains roughly the same, it is still a useful criterion. Additional theoretical data, discussed below, are available for even-mode resistance comparison.

The MININEC model shown in Fig. 9 is a simplified wire model which resulted from manipulating the diameter and position of a minimum number of wire elements to yield an impedance consistent with an effective height of 150 m, a static capacitance of 120 nF, and a resonant frequency of 38 kHz, which approximate both the North and South arrays. This model was analyzed with even- and odd-mode excitation. In subsequent comparison between the characteristics of this model and the actual reactance observed by PSR, an additional 6 nF of shunt capacitance was added at the input to bring the results into closer agreement. The MININEC impedance for a single array driven with the "off" array grounded is in close agreement with the measured impedance, with some discrepancy apparent with the lack of ohmic losses in the MININEC results as well as with the frequency of first resonance. Some discontinuities in the MININEC resistance curve are attributed to the relatively crude discretization employed in the approximate model. This should not invalidate the results for general comparison, however.

In the initial stage of this study it appeared that using two π-circuits with damping and coupling supplied by a circuit model of the TM01 spherical mode impedance (the impedance of the lowest order electromagnetic spherical mode generated by a monopole antenna [46]) would simulate the mutual

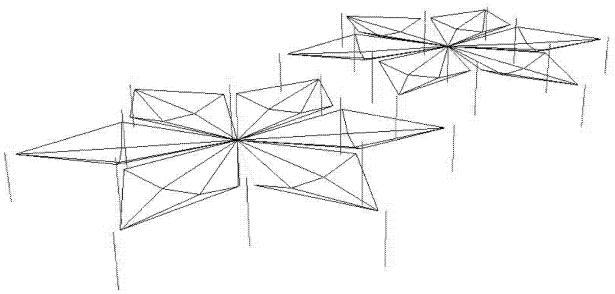

Fig. 9. Theoretical MININEC wire model.

coupling between the two arrays as well as with the radiated wave. The first target for simulation was to achieve an input resistance of approximately 0.27 Ω at 24 kHz for single-array operation, and 0.47 Ω at 24 kHz for dual-array operation [47]. In addition, the resistance and reactance profiles should reveal the same type of behavior as the measured data show, including the resonant frequency. These goals were not achieved after an extensive exercise of varying the available parameters. If a simple means of including mutual coupling using this π-circuit between arrays were available, this would be a simple solution for the model required. However, no satisfactory coupling network was discovered. At this point it was decided to try to achieve the desired results with a multisection ladder network.

Using MATHCAD, ladder networks similar to that shown in Fig. 10 were investigated using a wide variety of parameters. As these parameters were varied, several key results were monitored. 1) The single-array resistance at 24 kHz was steered to 0.27 Ω. 2) The even-mode resistance at 24 kHz was steered toward 0.47 Ω. 3) The rms deviations of the circuit R and X from the PSR R and X over the 10–40 kHz range were minimized separately for even-mode operation. 4) The rms deviations of the circuit R and X from the PSR R and X over the 10–40 kHz range were minimized separately for single-array operation. 5) The rms deviation of the circuit mutual resistance and reactance from the MININEC mutual resistance and reactance over the 10–40 kHz range were minimized separately.

How well these measures of circuit performance were achieved for the circuit of Fig. 10 is indicated in the following results. 1) The single-array resistance at 24 kHz achieved was 0.266 Ω (target 0.27 Ω). 2) The even-mode resistance at 24 kHz achieved was 0.488 Ω (target 0.47 Ω). 3) The rms deviations of the circuit R and X from the PSR R and X over the 10–40 kHz range were 0.0519 and 0.0663 Ω, respectively, for even-mode operation. 4) The rms deviations of the circuit R and X from the PSR R and X over the 10–40 kHz range were 0.0269 and 0.136 Ω, respectively, for single-array operation. 5) The rms deviations of the circuit mutual resistance and reactance from the MININEC mutual resistance

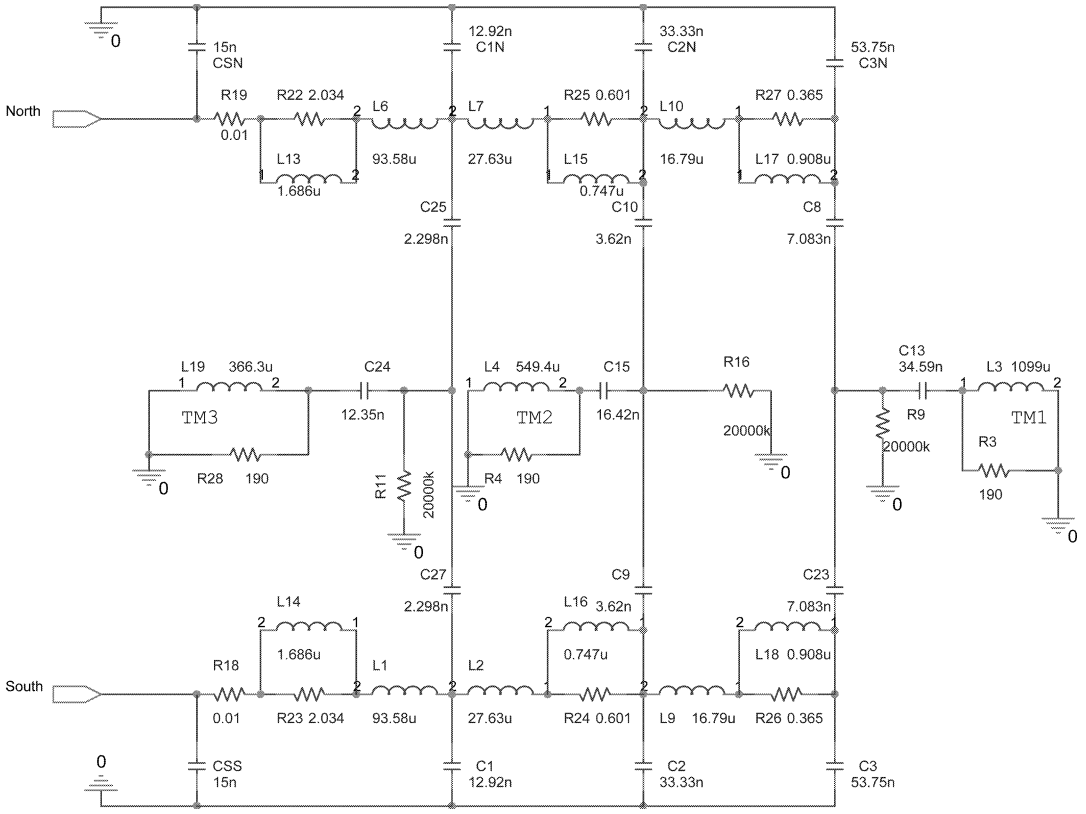

Fig. 10. PSPICE coupled antenna array model.

and reactance over the 10–40 kHz range were 0.00292 and 0.134 Ω, respectively. Figs. 11, 12, and 13 show comparisons of the resistance and impedance from the model of Fig. 10, the MININEC theory predictions, and the best available Cutler measured data.

A few preliminary coupling measurements were made at Cutler in 2000 [24], at the transmission line inputs. The South antenna tuning network was set to 100 Ω coupling and resonant at 23.9 kHz with the North antenna array grounded throughout the measurements. The North antenna array tuning network was then set with the South antenna array ungrounded, to 100 Ω coupling and resonant at various frequencies. With both antenna arrays ungrounded and disconnected from the combiner network, the South transmission line was terminated in a 100 Ω resistor, while the North transmission line was driven with a network analyzer at these frequencies. The amount of current induced in the terminating resistor on the South transmission line was measured and is an indication of the coupling between antenna arrays. The model defined by Fig. 10 exhibited a current of −27.7 dBc at 21.2 kHz, in contrast with our preliminary measurement of −41.7 dBc. Therefore this model appears to have more coupling than the Cutler arrays do, and the analysis performed in this report is conservative and places an upper limit on the distortion expected from Cutler.

The model in Fig. 10 used herein resulted from a fit to the data in both arrays. Future refinements to the model might include a small but measurable difference between North and South array.

VII. RESULTS

Harmonic distortion and IMD which is broadcast close to frequencies registered to Cutler and other U.S. VLF stations were of interest in this study. The frequencies registered to Cutler are: 14.1, 14.7, 14.8, 15.5, 17.8, 18.5, 18.6, 21.4, 21.425, 22.3, 22.35, 24.0, 25.3, and 25.82 kHz. Other U.S. VLF frequencies include: 19.8, 20.0, 24.8, 25.2, 26.8, 27.0, 27.5, 28.5, and 30.6 kHz. Of particular interest are the former and current Cutler broadcast frequencies (17.8 and 24.0 kHz). In our model, the North was run at 24.0 kHz and the South was run at 17.8 kHz, and upper limits on broadcast distortion were determined as presented below.

The AN/FRT-31 transmitter contains many tuned circuits that must be adjusted for each broadcast frequency. The procedure for tuning the model was more precise than the procedure for tuning the AN/FRT-31 in some ways and less precise in other ways. On the one hand, with a computer model it is possible to easily adjust network parameters to precise values needed for tuning, and a virtual network analyzer can be placed anywhere in the

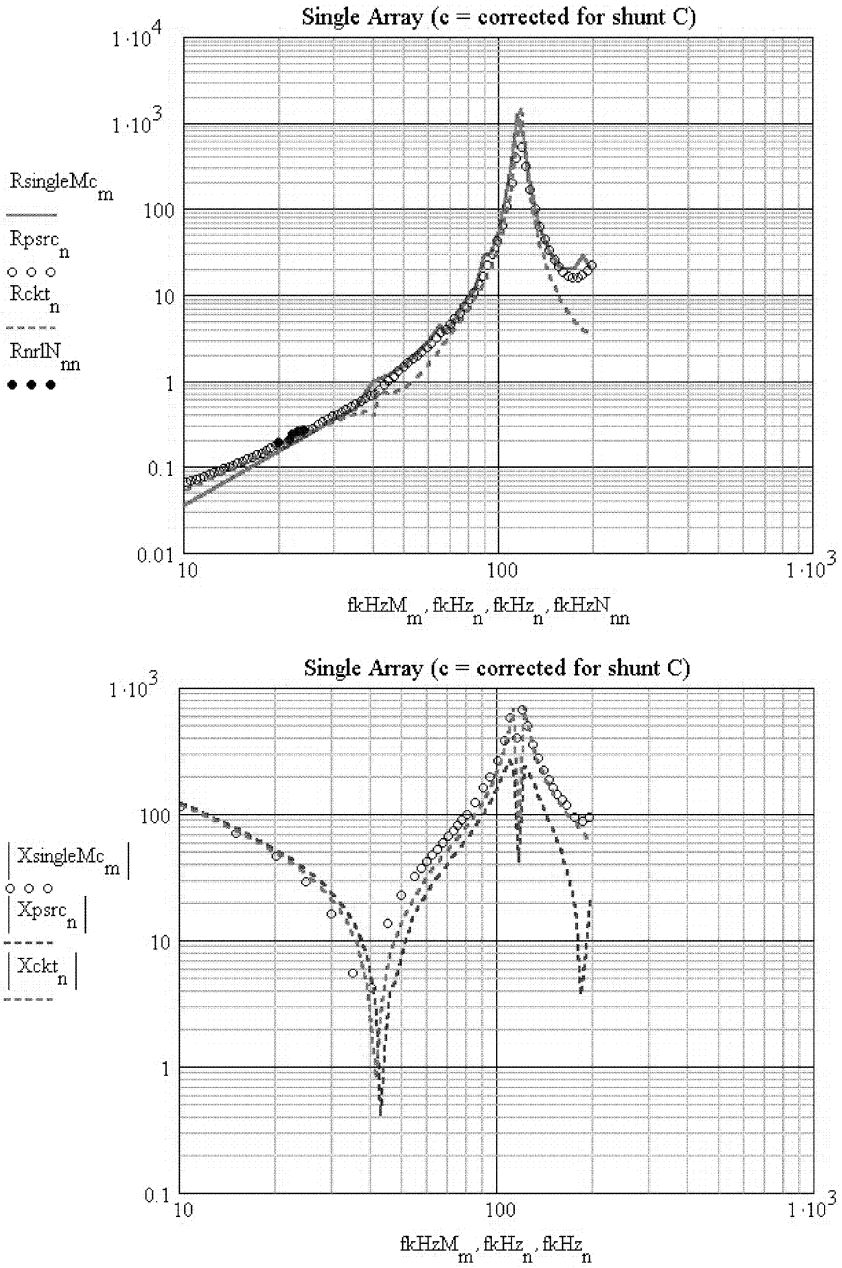

Fig. 11. Single-array resistance and reactance comparison: model, theory, and measurement.

circuit to check the coupling and resonance. On the other hand, it is more time consuming and laborious to adjust a simple tuning parameter in the model and test the effects than it is to tweak a control knob on the AN/FRT-31 until the desired criteria have been met. During the testing stage, attempts to tune the system for dual-array single frequency were relatively successful, however only single-array tuning was needed for the dual-frequency analysis. The procedure used to tune and run the model follows.

1) Select the frequency pair and modulation and assign North and South to each. For our choice and 200 baud modulation there are four combinations to run

North 24050 Hz, South 17850 Hz

North 24050 Hz, South 17750 Hz

North 23950 Hz, South 17850 Hz

North 23950 Hz, South 17750 Hz.

2) Determine the gross resistance value at each frequency from the antenna model by sweeping it and noting the value of Real(V/I) at those frequencies.

3) Set both North and South transmitter system components for those frequencies by calculation, including L_{coupling}, all the network components, and C_{plate} for each tank circuit.

4) Set the grid circuit capacitors and inductors for all four power amplifiers and both North

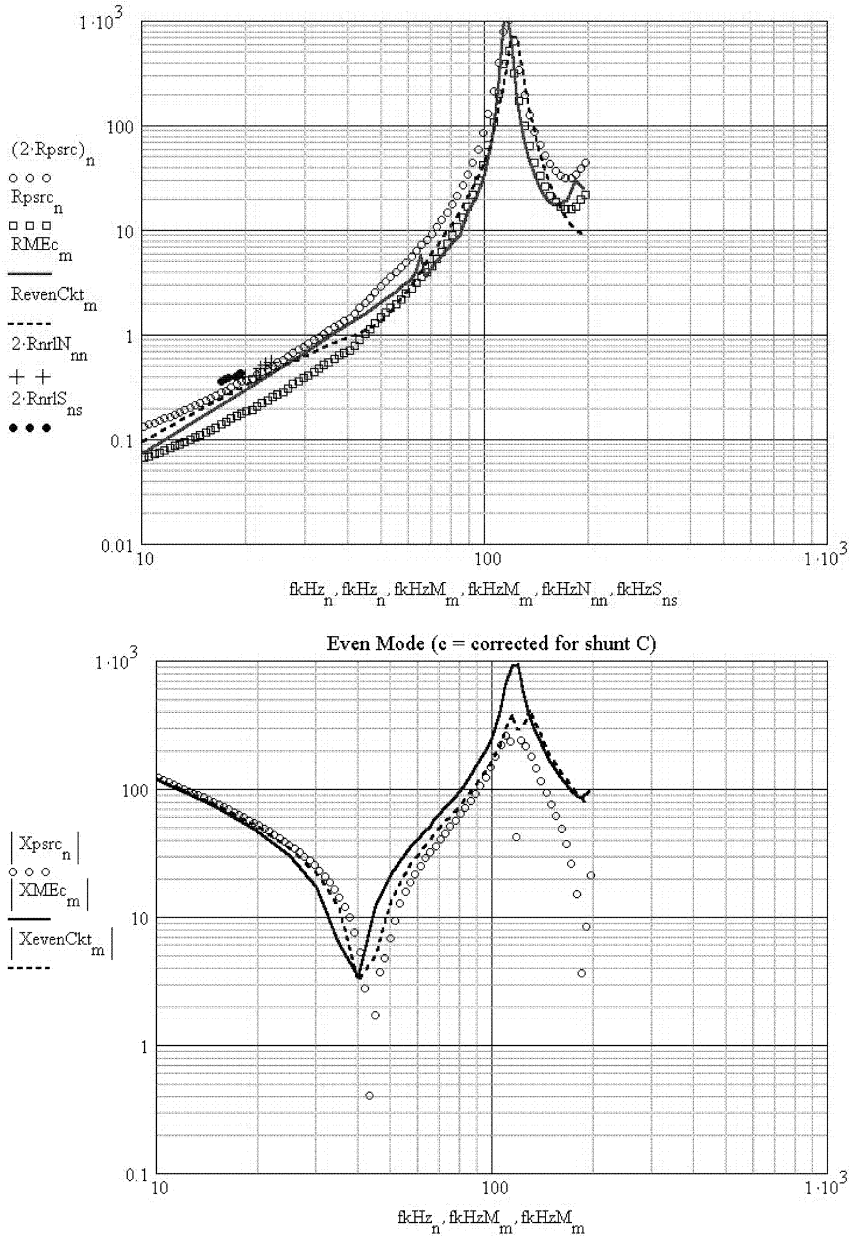

Fig. 12. Even-mode resistance and reactance comparison: model, theory, and measurement.

and South RF drives according to the respective frequencies.

5) Adjust L_{tune} in the North and South so that the helix house antenna tuning network inputs are $Z = 100 + j0$.

6) Check the plate-to-plate impedance in the North (by removing the filter circuit) so that it is symmetric at the modulated frequencies. Adjust the π-network components (phase shift) so that it is so.

7) Check the antenna current balance in the North at the modulated frequencies and adjust the network input reactance value so that it is symmetric.

8) Repeat step 6 and 7 for the South, adjusting the South network components.

9) Verify the North impedance, and antenna current balances are unaffected by step 8. For 24.0 and 17.8 kHz no change was observed.

10) Measure the IMD and harmonic distortion over 100 ms of data after the first 25 ms.

TABLE IV
Upper Limit Distortion Predictions

f (kHz)	I_{North} (dBc)	I_{South} (dBc)	f (kHz)	I_{North} (dBc)	I_{South} (dBc)
$f_1 = 23.95$	0	−38.9	$f_2 = 17.85$	−28.0	0
$2f_1 = 47.90$	< −108.6	< −102.0	$2f_2 = 35.70$	< −110.3	< −96.9
$3f_1 = 71.85$	−73.8	< −105.7	$3f_2 = 53.55$	−95.8	−57.0
$4f_1 = 95.80$	< −122.6	< −108.6	$4f_2 = 71.40$	< −119.8	< −105.9
$5f_1 = 119.75$	−105.9	< −110.6	$5f_2 = 89.25$	−111.0	−78.6
$6f_1 = 143.70$	< −126.3	< −112.4	$6f_2 = 107.10$	< −125.0	< −109.7
$7f_1 = 167.65$	−84.7	< −114.0	$7f_2 = 124.95$	−94.3	−80.1
$8f_1 = 191.60$	< −129.8	< −115.0	$8f_2 = 142.80$	< −124.9	< −112.6
$9f_1 = 215.55$	−102.2	−115.0	$9f_2 = 160.65$	−114.1	−90.2
$(2f_1 - f_2) = 30.05$	−78.3	−92.6	$(2f_2 - f_1) = 11.75$	−89.8	−87.4
$(3f_1 - 2f_2) = 36.15$	−102.0	−97.2	$(3f_2 - 2f_1) = 5.65$	−102.0	−98.9
f (kHz)	I_{North} (dBc)	I_{South} (dBc)	f (kHz)	I_{North} (dBc)	I_{South} (dBc)
$f_1 = 23.95$	0	−39.2	$f_2 = 17.75$	−28.1	0
$2f_1 = 47.90$	< −113.0	< −114.0	$2f_2 = 35.50$	−109.0	< −109.7
$3f_1 = 71.85$	−73.9	−113.6	$3f_2 = 53.25$	−104.8	−70.2
$4f_1 = 95.80$	< −121.5	< −124.5	$4f_2 = 71.00$	< −115.8	< −117.5
$5f_1 = 119.75$	−108.1	−117.7	$5f_2 = 88.75$	−115.2	−87.4
$6f_1 = 143.70$	< −124.0	< −126.6	$6f_2 = 106.50$	< −123.0	< −123.3
$7f_1 = 167.65$	−84.4	< −125.6	$7f_2 = 124.25$	−101.1	−87.3
$8f_1 = 191.60$	< −131.9	< −128.5	$8f_2 = 142.00$	< −128.1	< −127.7
$9f_1 = 215.55$	−102.9	< −129.1	$9f_2 = 159.75$	−121.4	−94.5
$(2f_1 - f_2) = 30.15$	−79.7	−98.2	$(2f_2 - f_1) = 11.55$	−85.6	−104.2
$(3f_1 - 2f_2) = 36.35$	−98.0	−108.4	$(3f_2 - 2f_1) = 5.35$	< −111.0	−105.8
f (kHz)	I_{North} (dBc)	I_{South} (dBc)	f (kHz)	I_{North} (dBc)	I_{South} (dBc)
$f_1 = 24.05$	0	−39.7	$f_2 = 17.75$	−27.8	0
$2f_1 = 48.10$	< −115.0	< −113.9	$2f_2 = 35.50$	< −107.5	−105.5
$3f_1 = 72.15$	−66.2	−112.6	$3f_2 = 53.25$	−110.5	−70.3
$4f_1 = 96.20$	< −117.3	< −121.8	$4f_2 = 71.00$	< −116.1	< −120.2
$5f_1 = 120.25$	−92.7	−108.1	$5f_2 = 88.75$	−117.4	−87.4
$6f_1 = 144.30$	< −123.9	< −124.7	$6f_2 = 106.50$	< −119.9	< −121.9
$7f_1 = 168.35$	−76.0	< −126.8	$7f_2 = 124.25$	−100.0	−86.3
$8f_1 = 192.40$	< −126.0	< −129.0	$8f_2 = 142.00$	< −123.8	< −123.4
$9f_1 = 216.45$	−87.1	−114.8	$9f_2 = 159.75$	−117.5	−94.6
$(2f_1 - f_2) = 30.35$	−81.1	−97.0	$(2f_2 - f_1) = 11.45$	−85.7	−99.8
$(3f_1 - 2f_2) = 36.65$	−98.7	< −109.2	$(3f_2 - 2f_1) = 5.15$	−106.4	−103.1
f (kHz)	I_{North} (dBc)	I_{South} (dBc)	f (kHz)	I_{North} (dBc)	I_{South} (dBc)
$f_1 = 24.05$	0	−39.4	$f_2 = 17.85$	−27.7	0
$2f_1 = 48.10$	< −110.6	< −102.6	$2f_2 = 35.70$	< −105.0	< −97.8
$3f_1 = 72.15$	−66.3	−105.3	$3f_2 = 53.55$	−97.5	−57.0
$4f_1 = 96.20$	−118.4	< −109.5	$4f_2 = 71.40$	< −116.5	−105.5
$5f_1 = 120.25$	−92.1	−103.7	$5f_2 = 89.25$	−112.0	−78.6
$6f_1 = 144.30$	< −124.3	< −113.7	$6f_2 = 107.10$	< −122.7	< −110.1
$7f_1 = 168.35$	−76.1	−113.5	$7f_2 = 124.95$	−93.3	−79.2
$8f_1 = 192.40$	< −128.4	< −116.2	$8f_2 = 142.80$	< −123.9	< −113.6
$9f_1 = 216.45$	−86.8	< −117.2	$9f_2 = 160.65$	−112.0	−90.3
$(2f_1 - f_2) = 31.15$	−82.3	−92.5	$(2f_2 - f_1) = 11.20$	−89.1	−88.4
$(3f_1 - 2f_2) = 36.45$	−79.9	−99.2	$(3f_2 - 2f_1) = 5.45$	−105.6	< −98.7

This procedure resulted in plate efficiencies of about 70%, in agreement with typical operation of the AN/FRT-31. The settling time is of the same order of magnitude as observed at Cutler. The harmonic currents observed in the antenna model are close to those observed at Cutler (see Section V). The plate current and plate supply voltage are set in the model to about the same values as in the AN/FRT-31, and the model results in roughly 500 kW per PA symmetric with modulation. For data collection times

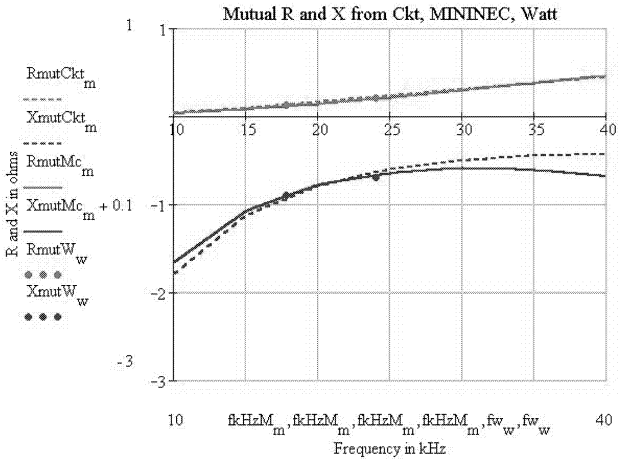

Fig. 13. Mutual resistance and reactance comparison: model, theory, and measurement.

of 100 ms, the noise levels were very low, allowing accurate measurements of the IMD and harmonic distortion products of interest. A step size of 1 μs was found to give convergent results as well as good resolution. After a transient analysis has run, PSPICE provides an FFT (Fast Fourier Transform) algorithm that calculates the spectra. In order to increase the frequency-domain resolution, longer data collection periods were used. A 100 ms span was found to give good resolution in the frequency domain without taking too long to calculate (about 1 hr on a 400 MHz Pentium II PC). Because the model behaves very much like the AN/FRT-31 and the calculation uncertainties in the model are small, the overall model was seen to be a good model for the Cutler VLF system. The most significant deviation from an ideal model is the overestimated antenna array coupling, which precludes predictions of high accuracy. However the distortion predictions made with this model are certainly accurate upper limits.

The IMD and harmonic distortion products of interest are f_1, $2f_1$, $3f_1$, $4f_1$, $5f_1$, $6f_1$, $7f_1$, $8f_1$, $9f_1$, f_2, $2f_2$, $3f_2$, $4f_2$, $5f_2$, $6f_2$, $7f_2$, $8f_2$, $9f_2$, $(2f_1 - f_2)$, $(2f_2 - f_1)$, $(3f_1 - 2f_2)$, and $(3f_2 - 2f_1)$. Table IV presents our distortion analysis results for dual-frequency operation. A "$<$" symbol indicates that the signal was not seen above that level. The design goal and current Navy specification for maximum harmonic distortion is -60 dBc, yet typical modern design requirements are set at -80 dBc. The Navy's maximum allowed IMD is -76 dBc.

The IMD upper limits in Table IV are less than -78 dBc, well below the Navy's maximum. The upper limits predicted for the harmonic distortions meet the Navy's limit of -60 dBc when averaged over modulation states. Because the harmonic distortion is due to the saturable core reactor ferrite material (see section V), dual-frequency mode operation does not introduce harmonic distortion at levels greater than what is already present in single-array mode. We conclude that the harmonic distortion and IMD for dual-frequency operation of the AN/FRT-31 at Cutler at the frequencies 17.8 and 24.0 kHz is low enough to allow operation in this configuration.

If NCTAMS LANT Det Cutler were to operate in dual-frequency mode, it is recommend that the metering equipment be modified to include frequency selectivity in order to reject the significant current induced at the fundamental frequency of the opposing array. This induced current is less than -28 dBc as seen in Tables I–IV. It is also recommended that the carrier cut-off system be modified so that the carriers are cut-off in both arrays whenever there is an arc in either array, so as to prevent the opposing array from feeding the arc and damaging the system.

ACKNOWLEDGMENTS

We would like to thank Russ Hammond of SPAWARSYSCEN San Diego for providing us with needed materials and help in generating a good model for the saturable reactors. We would also like to thank Andrew Grey for his help in checking equipment

settings at Cutler, which enabled us to make accurate models of the system components.

REFERENCES

[1] Continental Electronics Corporation (1998)
Technical Manual Operation and Maintenance for Radio Transmitter Set AN/FRT-31.
Continental Electronics Corporation, Sept. 29, 1998, revision 1.

[2] Roberts, M. A. (1989)
Trade study report NCU Cutler VLF combiner network improvements.
Electrospace Systems Report, SD89-066, Aug. 14, 1989.

[3] Gish, D.
Personal communication for help with the modeling and Cutler system and measurements at Cutler.

[4] Hansen, P. (1983)
VLF Cutler antenna measurements report.
Technical note 1245, Naval Electronics Systems Command, Jan. 1983.

[5] Gish, D. G. (2000)
Cutler/Holt synchronous tuner requirements analysis.
Pacific-Sierra Research Report, SD00722, contract N65236-99-D-5829, Dec. 1, 2000.

[6] ML-6696 ML-6697 General Purpose Triodes (1967)
Varian, ML-6696 ML-6697, Sept. 1967, 1.

[7] ML-6697 Description and Ratings (1955)
Machlett, ML-6697, June 1955, 1.

[8] Perugini, S, (2000)
Spice models for vacuum tubes (a survey).
Perugini Audio Engineering (PAENG) Italy, 2000.

[9] Perugini, S. (1998)
A low voltage phono preamp with T.H.D. cancellation.
Glass Audio, **10** (Feb. 1998).

[10] Koren, N. (1996)
Improved vacuum-tube models for SPICE simulations.
Glass Audio, **8**, 5 (May 1996), 18–27.

[11] Rydel, C. (1995)
Simulations of electron tubes with SPICE.
Audio Engineering Society Preprint 3965, AES Convention (G2), Paris, 1995.

[12] Leach, W. M., Jr. (1995)
SPICE models for vacuum-tube amplifiers.
Journal of Audio Engineering Society, **43**, 3 (Mar. 1995), 117–126.

[13] Reynolds, S. (1993)
Vacuum-tube models for PSPICE simulations.
Glass Audio, **5**, 4 (Apr. 1993), 17–23.

[14] Spangenberg, K. (1940)
Current division in plane-electrode triodes.
Proceedings of the IRE, **28** (May 1940), 226–236.

[15] Reisch, F.
Personal communication regarding earlier modeling work on the triode with PSR.

[16] Howard W. Sams & Co. (1975)
Reference Data for Radio Engineers.
Howard W. Sams & Co., 1975, 6-1–6-3.

[17] Jiles, D. C., and Atherton, D. L. (1986)
Theory of ferromagnetic hysteresis.
Journal of Magnetism and Magnetic Materials, **61** (1986), 48.

[18] Prigozy, S. (1993)
Pspice computer modeling of hysteresis effects.
IEEE Transactions on Education, **36**, 1 (Feb. 1993), 2.

[19] *OrCAD/Cadence Pspice manuals*.

[20] Hammond, R.
Personal communication for help with the reactor modeling from SPAWARSYSCENSANDIEGO.

[21] Cutler synchronous tuner assessment test results.
Electrospace Systems Report SD88-081, Aug. 17, 1988.

[22] Gish, D. G., and Hopkins, W. D. (2000)
VLF Cutler maximum power and north antenna six/four panel test results.
Pacific-Sierra Research Report, SD00-669, June 30, 2000.

[23] Beauchamp, E. T., Hopkins, W. D., and Gish, D. G. (1998)
AN/FRT-31, VLF Cutler six and four panel test results south array.
Pacific-Sierra Research Report, SD97-546, Jan. 30, 1998.

[24] Hopkins, W.
Personal communication for providing measurement data of Cutler.

[25] Tolonen, J. (1997)
High performance tubed DAC output stage, Part 1.
Megabaud Finland, Aug. 24, 1997.

[26] Review of particle physics for statistical analysis techniques.
European Physical Journal, **C3**, 1 (1998), 1233.

[27] Simpson, T. L. (1979)
Computer simulation of VLF power amplifiers under reactive loading.
IEEE Transactions on Aerospace and Electronic Systems, **AES-15**, 5 (Sept. 1979), 683.

[28] Luro, M., and Gray, A.
Personal communication for help with measurements of the PA and tank circuits at Cutler.

[29] Condon, E. U., and Odishaw, H. (Eds.) (1967)
Handbook of Physics (2nd ed.).
New York: McGraw-Hill, 1967.

[30] Coaxial transmission line technical data.
Andrew Catalog 38, Heliax Coaxial Cables, 2000, 631.

[31] Intermodulation Generation.
Andrew Catalog 38, Heliax Coaxial Cables, 2000, 630.

[32] Henney, K. (Ed.) (1959)
Radio Engineer's Handbook (5th ed.).
New York: McGraw-Hill, 1959.

[33] King, R. W. P., Mimno, H. R., and Wing, A. H. (1945)
Transmission Lines Antennas and Waveguides.
New York: McGraw-Hill, 1945, 4–29.

[34] Chretien, N. (1998)
Lossless transmission line computation tutorial.
Hworcester Polytechnic Institute, Dept. of Electrical and Computer Engineering, EE535 course, homework solution set #2, Spring 1998.

[35] Raudenbush, J. E. (1976)
NRL tech memo 5460-101A, Mar. 8, 1976.

[36] Hirasuna, B. (1999)
Using coupled inductors and inductor cores.
OrCad Pspice Application Note #PSPA021, Apr. 1999.

[37] Hirasuna, J., and Hirasuna, B.
OrCAD/Cadence Pspice Tech Support staff.

[38] Thomas, B. (2000)
A fresh look at nonlinear distortion theory in inductors.
RF Design, (Jan. 2000), 28.

[39] Snoek, J. L. (1946)
Non-metallic magnetic material for high frequencies.
Philips Technical Review, **8**, 12 (Dec. 1946), 353.

[40] Beljers, H. G., and Snoek, J. L. (1950)
Gyromagnetic phenomena occuring with ferrites.
Philips Technical Review, **11**, 11 (May 1950), 313.

[41] Went, J. J., and Gorter, E. W. (1952)
The magnetic and electrical properties of ferroxcube materials.
Philips Technical Review, **13**, 7 (Jan. 1952), 181.

[42] *Reference Data for Radio Engineers* (3rd ed.).
ITT, 1949, 193–196.

[43] Compressed powdered molybdenum-permalloy for high-quality inductance coils.
Bell System Technical Journal, **19** July 1940, 385.

[44] Raudenbush, J. E. (1972)
Antenna radiation characteristics for the Navy VLF transmitting stations NAA, NBA, and NDT.
NRL tech memo 2439, May 1972.

[45] Watt, A. D., and Smith, C. E. (1984)
Technical report tune condition definition: NRTF Cutler.
Electrospace Systems Report for NOSC, Aug. 15, 1984.

[46] Harrington, R. (1961)
Space as a waveguide.
Time-Harmonic Electromagnetic Fields. New York: McGraw-Hill, ch. 6, sect. 6-4, 1961.

[47] Simpson, T. L., Fenwick, R. C., and Matlack, N. C. (1976)
Final report Verdin integration tests at VLF Cutler.
Electrospace Systems Report, ER-76-06U, May 28, 1976.

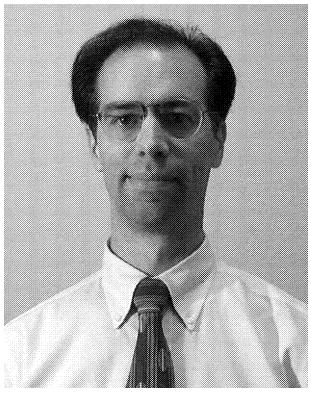

Eric C. Berg received the Ph.D. degree in high energy physics from the University of California, Los Angeles in 1994.

He held a postdoctoral position in low temperature physics at the University of California, San Diego, and was then employed as an RF systems engineer from 1996 to 2001 where he performed various development and service tasks on large VLF, LF, and ELF transmitter systems. He is currently pursuing research in gravitational physics at the University of California, Irvine.

Michael A. Roberts (M'78—SM'01) received the B.E.E. degree from the University of Delaware, Newark, in 1977.

From 1977 to 1984 he was employed at General Dynamics where he designed and analyzed electrical, instrumentation, and RF systems for space launch vehicles. Since 1984 he has been engaged in design, development, analysis, commissioning, and field test of high-power radio broadcast systems for long-range communications applications in the ELF, VLF, and LF bands.

Mr. Roberts is a registered professional engineer in the state of California, a NARTE certified EMC engineer, and an affiliate member of the International Electrical Testing Association.

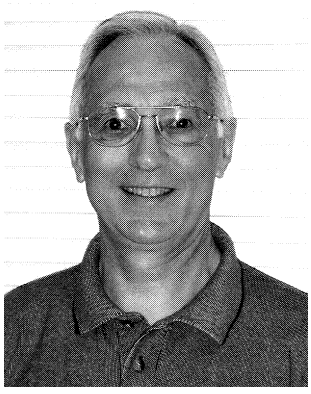

Ted L. Simpson (S'55—M'56—SM'70—LS'99) received the B.S.E.E. degree in 1956 and the M.S. degree in 1959 from the University of Tennessee, Knoxville, and the Ph.D. degree from Harvard University, Cambridge, MA in 1970.

From 1956 to 1967 he was employed by Deco Electronics in Leesburg, VA. He has been with the Department of Electrical Engineering at the University of South Carolina since 1968.

Dr. Simpson is a registered professional engineer in the state of South Carolina.